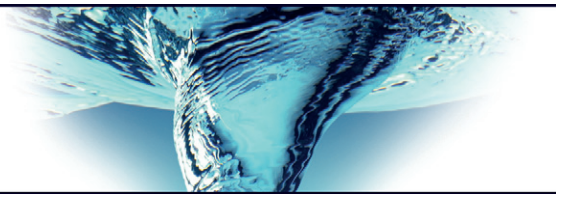
J. Fluid Mech. (2016), *vol.* 804, R6, doi:10.1017/jfm.2016.575



JFM RAPIDS
journals.cambridge.org/rapids

Transition to turbulence over 2D and 3D periodic large-scale roughnesses

A. M. Hamed[1], M. Sadowski[1], Z. Zhang[1] and L. P. Chamorro[1,2,3,†]

[1]Department of Mechanical Science and Engineering, University of Illinois, Urbana, IL 61801, USA

[2]Department of Civil and Environmental Engineering, University of Illinois, Urbana, IL 61801, USA

[3]Department of Aerospace Engineering, University of Illinois, Urbana, IL 61801, USA

(Received 21 June 2016; revised 27 August 2016; accepted 28 August 2016; first published online 8 September 2016)

A laboratory investigation was performed to study distinctive features of the laminar-to-turbulent transition over distributed roughness characterized by two-dimensional (2D) and three-dimensional (3D) periodic, low-order topographies at roughness Reynolds number $Re_k \approx 300$. Systematic experiments were performed using high-spatial-resolution planar particle image velocimetry (PIV) in a refractive-index-matching (RIM) channel, where the roughness covered the entire length of the test section. The results show that the flow over the 2D roughness becomes turbulent much sooner than its 3D counterpart ($Re_x = 50\,000$ versus $120\,000$). This is attributed to the presence of a velocity inflection point resulting from flow separation within the troughs of the 2D roughness. In the transitional region, unsteady disturbances above the two roughnesses appear upstream of near-roughness disturbances. The above-roughness disturbances are associated with the inflection point in the vertically displaced boundary layer for the 2D case, and with the mean velocity deficit resulting from the interaction of the wakes of upstream elements for the 3D case. The near-roughness fluctuations are associated with the shear layer present behind the crests of both roughnesses. The transitional region is characterized by the interaction between above- and near-roughness disturbances, which merge, leading to a rapid vertical growth of the turbulent fluctuations.

Key words: instability, transition to turbulence

1. Introduction

Roughness-induced transition has been a subject of extensive study dating back to the 1940s (Dryden 1953). Understanding the role of roughness in flow transition is

† Email address for correspondence: lpchamo@illinois.edu

© Cambridge University Press 2016

https://doi.org/10.1017/jfm.2016.575 Published online by Cambridge University Press

essential for prediction and design, as well as flow control and drag reduction through the delay of the turbulent transition (Cossu & Brandt 2002; Choi 2006; Fransson *et al.* 2006). Early works focused on the roughness Reynolds number $Re_k = U_k k/\nu$ as a characteristic parameter in determining the transition (e.g., Klebanoff, Schubauer & Tidstrom 1955; Smith & Clutter 1959); here, U_k denotes the velocity at the roughness height (k) and ν is the kinematic viscosity. Further distinctions are based on whether the roughness is two-dimensional (2D) or three-dimensional (3D), and whether it is distributed or isolated. In terms of Re_k, the transition to turbulence is expected to occur downstream of the roughness element at a critical threshold $Re_{k,crit}$. Moreover, a 3D roughness is identified as more critical than a 2D one, meaning that when $Re_{k,crit}$ has been exceeded, the transition location will rapidly approach the roughness element (Tani 1969). Below $Re_{k,crit}$, it was believed that 3D roughness has an insignificant effect on the flow transition (Klebanoff *et al.* 1955; Tani 1969).

As discussed by Klebanoff & Tidstrom (1972), Ergin & White (2006), Kuester & White (2015) and others, the Re_k criterion falls short in explaining the underlying physics of the transition process. Understanding roughness-induced transition is an essential prerequisite to the use of roughness as a control mechanism to reduce skin friction by delaying the flow transition, as proposed by Shahinfar *et al.* (2012, 2013) and others. For discrete 2D roughness, the transition is explained by the 2D Tollmien–Schlichting (T–S) waves (Klebanoff & Tidstrom 1972; Goldstein 1985). The need for further understanding of the effect of 3D roughness on flow transition has motivated many recent studies, including Bernardini *et al.* (2014), Plogmann, Würz & Krämer (2014), Edelmann & Rist (2015) and Ye, Schrijer & Scarano (2016), to name a few. Transient growth, a candidate mechanism explaining bypass transition over 3D isolated and distributed roughness, emerges due to the non-orthogonality of the linear stability equations (Reshotko 2001; Reshotko & Tumin 2004; Downs, White & Denissen 2008). Essentially, it is described by the combination of slightly decaying modes, resulting in transient growth followed by exponential decay (Reshotko & Tumin 2004; Kuester & White 2015).

Recent works have focused on the flow in the near and far wake of 3D isolated roughness elements. Ergin & White (2006), for example, studied the flow past an array of cylindrical elements at subcritical and supercritical Re_k. In addition to providing evidence of hairpin vortices, they highlighted that the transition occurs when the field of the unsteady disturbance (velocity fluctuations) grows rapidly such that the altered steady flow cannot relax fast enough to stabilize the fluctuations. As such, roughness-induced transition could be thought of as a competition between these two factors. Recently, Ye *et al.* (2016) experimentally investigated the transition past a micro-ramp at a supercritical $Re_k = 1170$ using tomographic particle image velocimetry (PIV) and highlighted the shedding of arc-like Kelvin–Helmholtz (K–H) vortices. Past the breakup of the arc-like vortices, a region of relatively low vortical activity was observed, followed by the development of hairpin vortices near the wall, indicating flow transition.

The role of distributed roughness in flow transition remains a challenging topic in need of further investigation, especially due to its relevance as a realistic wall condition. Downs *et al.* (2008) studied the flow transition past a patch of random distributed roughness at $Re_k = 164$, 227 and 301. They observed transient growth in the steady disturbances (deviations from the Blasius profile due to the generated wakes) across the three Re_k, and suggested that the transition at the high Re_k occurs through bypass mechanisms. Moreover, they observed a similar competition between the relaxation of steady disturbances (stabilizing effect) and the growth of the fluctuations

https://doi.org/10.1017/jfm.2016.575 Published online by Cambridge University Press

as in Ergin & White (2006). Direct numerical simulations (DNS) of the flow past the same roughness were performed by Drews *et al.* (2011) and Drews (2012) to further understand the nature of the transition. A key finding in these works is that the regions with the largest roughness heights were responsible for the majority of the distortion of the initially undisturbed boundary layer. Additionally, Drews (2012) suggested that the small roughness acts as a 'shield' where the boundary layer gets displaced vertically over the small-scale roughness, thus shielding the larger roughness elements through a lower effective Re_k. Because of the importance of such an effect, Kuester & White (2015) performed systematic experiments to investigate the nature of the interaction between distributed roughness and isolated elements. They found that sheltering is not fully explained by boundary layer displacement as suggested by Drews (2012).

The works of Downs *et al.* (2008) and Kuester & White (2015) pointed out the need for a characterization of flow transition over long patches of distributed roughness. Our study aims to contribute to satisfying this need within the rapidly evolving field of roughness-induced transition. Here, we consider the transition to turbulence over 2D and 3D wavy walls. The flow over these roughnesses in the regime of developed turbulence has been studied by Hamed *et al.* (2015), who found that 3D roughness led to reduced drag in comparison to the 2D case. This reduction was attributed to the characteristic spanwise flows within the 3D wall, which provide high momentum in the wakes of the 3D 'hills'. Here, we provide quantitative evidence of the distinctive transition to turbulence behaviour over 2D and 3D distributed roughness that spanned the entire length of the test section. This set-up provides information regarding the transition over roughness which complements and advances previous works that studied the flow transition past a short patch of roughness. The experimental set-up is described in § 2, the results are presented and discussed in § 3, and concluding remarks are presented in § 4.

2. Experimental set-up

Highly controlled experiments were carried out to capture the laminar-to-turbulent transition over 2D and 3D wavy walls. The measurements were made with planar PIV in a 2.5 m long refractive-index-matching (RIM) channel with a 112.5×112.5 mm^2 cross-section. The 2D roughness is described by a single sinusoidal wave in the streamwise direction with a ratio of amplitude to wavelength $a/\lambda_x = 0.05$, while the 3D roughness is defined with an additional wave superimposed on the 2D wall in the spanwise direction with $a/\lambda_y = 0.1$. The surface topography $\sigma(x, y)$ of both walls is illustrated in figure 1. The effect of this roughness on the boundary layer in the regime of developed turbulence at Reynolds number $Re = 4 \times 10^4$ (based on the bulk velocity and channel half-height) was studied by Hamed *et al.* (2015). They highlighted the advantage of such model in identifying the impact of the three-dimensionality of roughness on turbulent boundary layers. Both roughnesses are 'distributed' in the sense that they are periodic and consist of multiple peaks and troughs. Moreover, the roughness is of low order such that all peaks and troughs have the same height. For the purpose of refractive index matching, the walls were cast from urethane resins using hydrodynamically smooth moulds. NaI aqueous solution ($\sim$63 % by weight, $\rho = 1800$ kg m^{-3}, $\nu \sim 1.1 \times 10^{-6}$ m^2 s^{-1}) was used as the working fluid. Through careful temperature control, the refractive index of the solution was fine-tuned to match that of the wall, rendering it nearly invisible. RIM allowed for measurements very close to the walls and within the troughs of the 3D roughness.

https://doi.org/10.1017/jfm.2016.575 Published online by Cambridge University Press

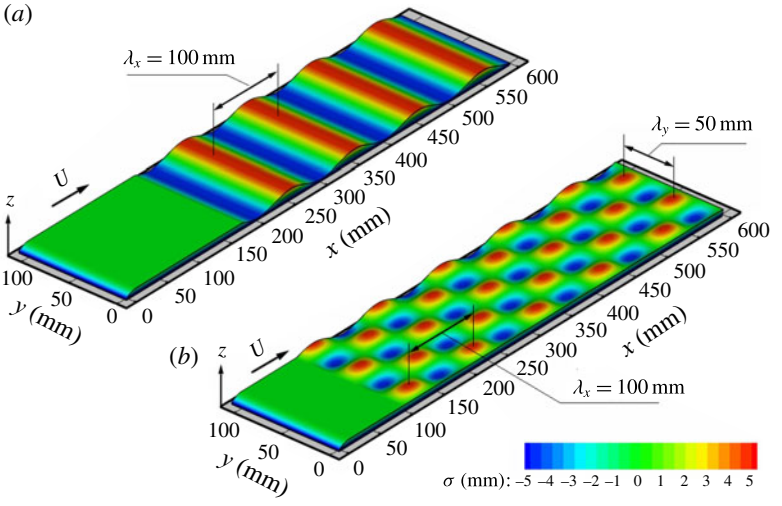


FIGURE 1. A section of the 2D (*a*) and 3D (*b*) walls illustrating the topography of each roughness. Also shown is the elliptical inlet and the short preceding flat plate.

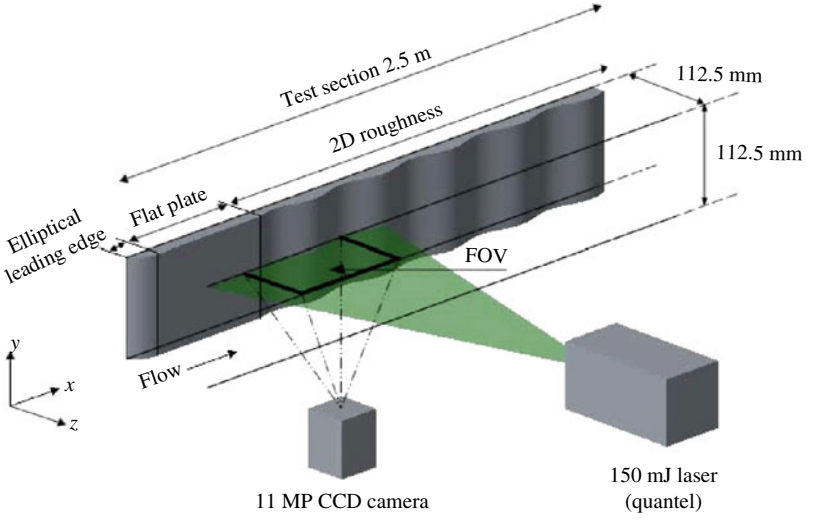


FIGURE 2. Schematic of the experimental set-up illustrating a section of the channel with the 2D roughness, and one of multiple fields of view (FOV).

The flow measurements were made in a streamwise wall-normal (x–z) plane with a spanwise location corresponding, approximately, to the channel centre (figure 2). A planar PIV system consisting of an 11 MP (4000×2672 pixels) CCD camera and a 150 mJ pulse^{-1} double-pulsed laser was used, resulting in a final vector grid spacing $\Delta x = \Delta z = 300$ μm. Figure 2 shows the general schematics of the experimental set-up. The PIV system and technique used here are similar to those of Hamed *et al.* (2015); the reader is referred to Blois *et al.* (2012) and Bai & Katz (2014) for additional details on the channel and the RIM technique.

https://doi.org/10.1017/jfm.2016.575 Published online by Cambridge University Press

The roughnesses were preceded by a short flat plate with an elliptical leading edge (0.18 m for the 2D and 0.1 m for the 3D). In order to capture the location of flow transition and the flow behaviour leading to it, flow measurements over the 2D wall were made in six consecutive fields of view (FOV) extending from the entrance region to $x/\lambda_x = 8.5$. For the 3D roughness, flow measurements are reported in three FOVs around the location of the turbulent transition, which was found with exploratory measurements. The flow transition was studied under a free-stream velocity of $U_\infty = 0.09$ m s^{-1}, yielding a Reynolds number based on the channel half-height $Re_h = 4600$. The roughness Reynolds number is $Re_k = U_k k/\nu = 323$ and 341 for the 2D and 3D roughnesses, where k is taken as the amplitude of the roughness. The ratio of roughness height to thickness of the incoming boundary layer is $k/\delta_{99} = 0.56$ and 0.6 for the 2D and 3D models. To gain further insight, the flow field over the 3D roughness was characterized at five other free-stream velocities spanning the range 0.07–0.15 m s^{-1}. For both roughnesses, 2000 PIV realizations were collected in each FOV. The small difference in the flat-plate length preceding the two roughnesses did not lead to significant differences as seen in Re_k and k/δ_{99}. The Re_k is comparable to that of Downs *et al.* (2008) and Kuester & White (2015) for the flow transition past a patch of distributed roughness. The relatively large amplitude of the roughness allows for spatially well-resolved measurements within it. However, it is important to note that, given this relatively large roughness height, the geometry of the roughness becomes a key component in defining the flow and, as such, the topography is referred to as large-scale roughness. In the literature, the effect of k/δ_{99} on the transition to turbulence is mostly encompassed in Re_k. Further investigation of this effect is needed and it is the subject of current research (e.g., Bernardini *et al.* 2014). Finally, it is noteworthy that preliminary experiments over a smooth flat wall and under the same flow conditions indicated that the undisturbed flow remained laminar across the entire length of the test section.

3. Results and discussion

3.1. *Transition to turbulence over the 2D roughness*

To characterize the transition to turbulence over the distributed 2D roughness, we performed extensive high-spatial-resolution PIV measurements covering a length of 0.7 m. The time-averaged distributions of the streamwise U/U_∞ and wall-normal W/U_∞ velocity components over this length are illustrated in figure 3. There, selected 1D profiles are also included to highlight the evolution of the mean flow. The incoming laminar boundary layer separates within the troughs, creating a region of reversed flow, which is marked with the blue dashed line in figure 3(*b*). This region occupies the majority of the second and third troughs; however, it significantly reduces downstream, where the flow begins the transition to turbulence. As shown below in figure 5, the flow is in the transitional regime within $4 \lesssim x/\lambda_x \lesssim 6$ and becomes turbulent at $\sim 6\lambda_x$ or 0.6 m from the leading edge ($Re_x = U_\infty x/\nu = 5 \times 10^4$). In the laminar region ($x/\lambda_x \lesssim 4$), the roughness seems to have a comparatively less significant role in modulating the flow, as suggested by the distribution of the vertical velocity W/U_∞. A region of comparatively high upward flow occurs at the first roughness peak; otherwise the wall-normal velocity is significantly lower than that within the turbulent region $x/\lambda_x \gtrsim 6$ (figure 3*c*). A negligible flow of momentum occupies the majority of the troughs within the laminar region and results in the upward displacement of the boundary layer. Drews (2012), in his DNS study of 3D distributed roughness, replaced the troughs with a streamwise and spanwise

https://doi.org/10.1017/jfm.2016.575 Published online by Cambridge University Press

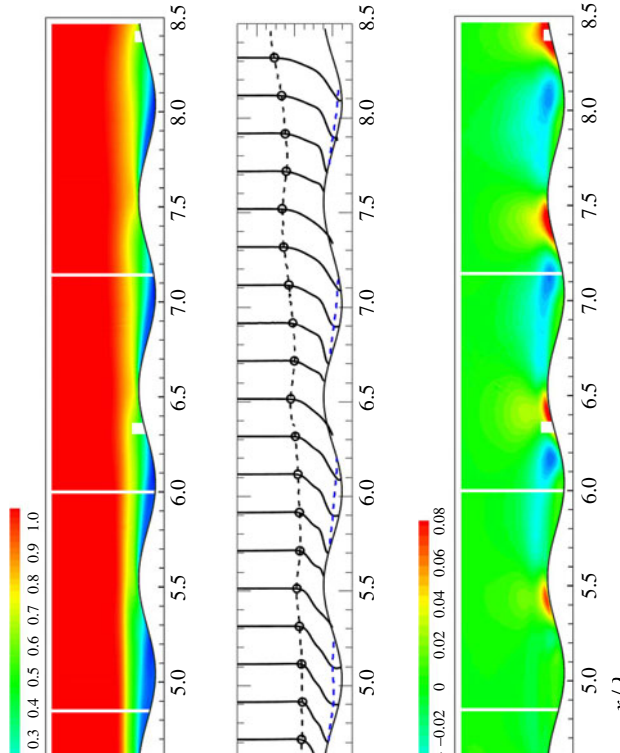


FIGURE 3. Contours (*a*) and profiles (*b*) of the time-averaged streamwise velocity U/U_∞ over the 2D roughness. The white vertical strips outline the different FOVs. The dashed black line denotes δ_{99}/H and highlights the growth of the boundary layer. The dashed blue line indicates a contour line where $U = 0$. (*c*) Contours of the time-averaged wall-normal velocity W/U_∞. The small rectangular regions at the wall are due to optical obstacles outside the test section.

https://doi.org/10.1017/jfm.2016.575 Published online by Cambridge University Press

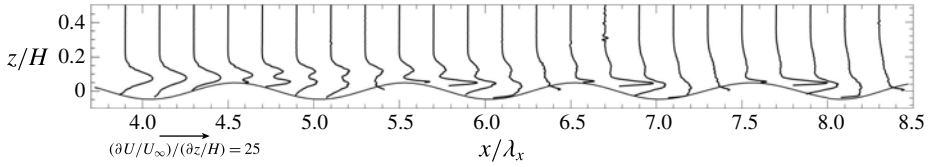


FIGURE 4. Mean shear $\partial(U/U_\infty)/\partial(z/H)$ over a section of the 2D roughness covering the transitional and turbulent regions.

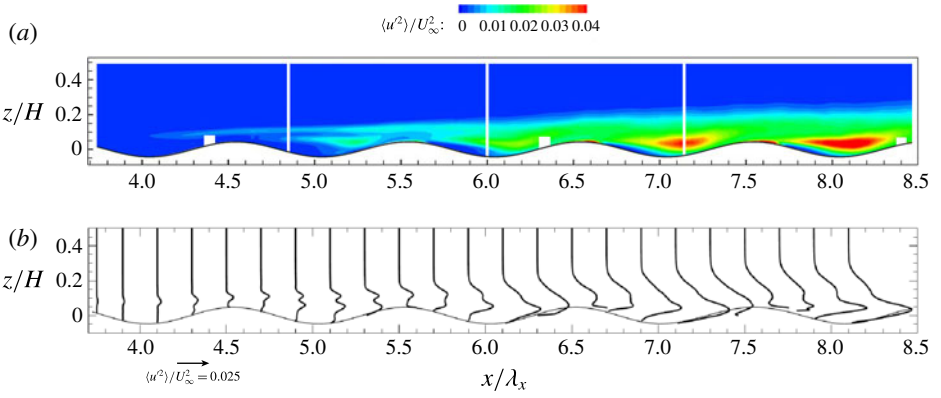


FIGURE 5. Contours (*a*) and profiles (*b*) of the streamwise velocity variance $\langle u'^2\rangle/U_\infty^2$ over a section of the 2D roughness covering the transitional and turbulent regions.

slip surface to understand the effect of roughness 'valleys'. He found that the flow downstream is unaffected, and suggested that roughness valleys do not significantly contribute to receptivity. A somewhat similar behaviour is observed here for the 2D roughness, where the recirculation within the valleys in the laminar regime ($x/\lambda_x \lesssim 4$) acts as a blockage, reducing wall-normal flows and possibly minimizing vortical shedding from the 2D hills.

However, a major difference from the work of Drews (2012) is the disturbances created by the separated flow within the 2D roughness troughs. The recirculation region enables an inflection point in the boundary layer profile that corresponds to a maximum in the mean shear $\partial(U/U_\infty)/\partial(z/H)$ shown in figure 4. For $x/\lambda_x \lesssim 4.5$, the boundary layer profile exhibits an inflection point with a mean shear maximum that is thought to promote flow instability, leading to the peak in the streamwise velocity variance $\langle u'^2\rangle/U_\infty^2$, which is shown, for clarity, as contours and profiles in figure 5. This quantity reveals that the region $x/\lambda_x \lesssim 4$ has negligible fluctuations and is identified as the laminar regime, whereas for $x/\lambda_x \gtrsim 6$ the flow exhibits spatially distributed turbulent fluctuations similar to that observed by Hamed *et al.* (2015) in a developed flow, and is thus identified as the turbulent regime. There, the production of turbulence is attributed to the shear layer formed behind the roughness crests. The intermediate zone $4 \lesssim x/\lambda_x \lesssim 6$ is considered, consequently, to be a transitional region. Within this zone, the fluctuations are contained in a narrow band ($4 \lesssim x/\lambda_x \lesssim 4.7$) above the roughness with peak at $z/H = 0.08$–0.1 coincident with a peak in the mean shear associated with the mean velocity inflection. The fluctuations in this region possibly trigger disturbances near the roughness. The crest near $x/\lambda_x = 4.5$ develops a shear layer, which leads to additional velocity inflection points that

https://doi.org/10.1017/jfm.2016.575 Published online by Cambridge University Press

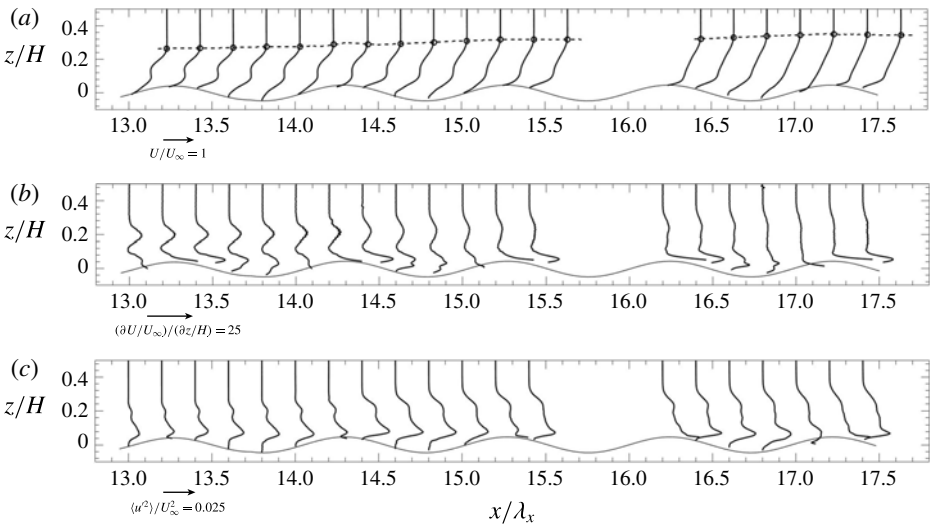


FIGURE 6. (*a*) Profiles of time-averaged streamwise velocity U/U_∞ over a section of the 3D roughness. The dashed black line denotes δ_{99}/H. (*b,c*) The corresponding profiles of the mean shear $\partial(U/U_\infty)/\partial(z/H)$ and the streamwise velocity variance $\langle u'^2\rangle/U_\infty^2$.

explain the two shear and velocity variance peaks observed within the transitional region (figures 4 and 5). The near-roughness fluctuations quickly over take those related to the displaced boundary layer. However, in the transitional region the two mechanisms interact and lead to rapid vertical growth of the velocity fluctuations.

3.2. *Transition to turbulence over the 3D roughness*

The characterization of the transition to turbulence over the distributed and low-order 3D roughness provides important insight into the case where the steady disturbances (wakes) are created over an array of compact elements covering the entire domain. This advances the work of Downs *et al.* (2008) and Kuester & White (2015), who studied the downstream evolution of disturbances created over a short roughness patch. Moreover, due to the similar experimental conditions, free-stream velocity $U_\infty = 0.09$ m s^{-1} and $Re_k \approx 300$, the results presented here provide a meaningful comparison between flow transition over the periodic 2D and 3D roughnesses. The flow over the 3D roughness reaches its turbulent behaviour at 1.5 m ($Re_x = 1.2 \times 10^5$) from the leading edge in comparison with 0.6 m ($Re_x = 5 \times 10^4$) for the 2D wall, i.e., 2.5 times longer. Therefore, we focus on the mean streamwise velocity U/U_∞, the mean shear $\partial(U/U_\infty)/\partial(z/H)$ and the streamwise velocity variance $\langle u'^2\rangle/U_\infty^2$ within the transitional and turbulent regions, which are shown in figure 6. The lack of mean flow reversal within the troughs is due to the preferential flows identified by Hamed *et al.* (2015), which inject momentum into the wakes of the 3D hills. The flow field is best analysed in the context of the work by Ergin & White (2006), Downs *et al.* (2008) and Kuester & White (2015). There, it is shown that, as the undisturbed boundary layer flow passes roughness elements, the formed steady disturbances (wakes) lift up downstream, experience transient growth and promote velocity fluctuations. The transition to turbulence occurs when the fluctuations grow rapidly before the unstable steady state can relax to a stable one. Here, the process

https://doi.org/10.1017/jfm.2016.575 Published online by Cambridge University Press

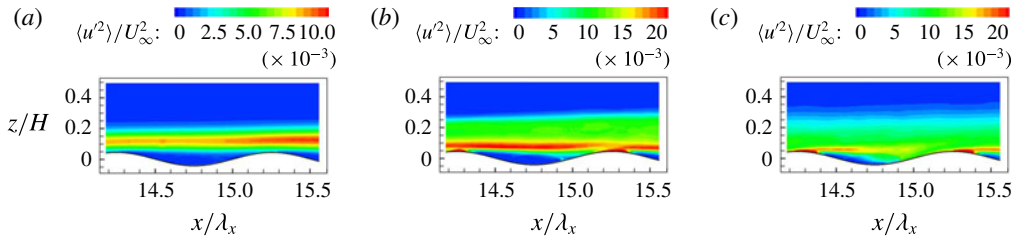


FIGURE 7. Contours of the streamwise velocity variance $\langle u'^2\rangle/U_\infty^2$ for the 3D wall at $14.2 \leqslant x/\lambda_x \leqslant 15.5$ for different free-stream velocities. (*a*) $U_\infty = 0.07$ m s^{-1}, (*b*) $U_\infty = 0.09$ m s^{-1}, (*c*) $U_\infty = 0.16$ m s^{-1}.

is different because steady disturbances (wakes) are generated along the entire flow domain at each element of the roughness array. These steady disturbances lift up and likely interact over the length of the roughness array, leading to the mean velocity deficit at $0.08 \lesssim z/H \lesssim 0.25$ (figure 6*a*). Consequently, it is challenging to uncouple the contribution of the generation from the growth/decay. Therefore, the systematic velocity deficit observed in figure 6(*a*) is an aggregation of both.

The velocity deficit at $0.08 \lesssim z/H \lesssim 0.25$ (figure 6) corresponds to a region of enhanced shear and fluctuations with local peaks near $z/H = 0.2$. High mean shear and comparatively larger velocity fluctuations are also induced near the roughness. These fluctuations overtake those related to the steady disturbances. However, they interact similarly to the 2D case, leading to rapid vertical growth of the fluctuation distribution. The steady disturbances and their corresponding shear rapidly decay due to turbulent mixing at $x/\lambda_x \gtrsim 15$. To further highlight the effect of this interaction, we show in figure 7 contours of the streamwise velocity variance $\langle u'^2\rangle/U_\infty^2$ in the region $14.2 \leqslant x/\lambda_x \leqslant 15.5$ for three free-stream velocities ($U_\infty = 0.07$ m s^{-1}, $U_\infty = 0.09$ m s^{-1}, $U_\infty = 0.16$ m s^{-1}). When considering the location of flow transition, the lower (higher) free-stream velocity is somewhat analogous to moving the measurement region upstream (downstream). At the lowest velocity, only the fluctuations associated with the steady disturbances are present. At the highest velocity, the flow is in its turbulent regime where the turbulence is generated by the shear layer downstream of the hills, similar to the findings of Hamed *et al.* (2015). The case with $U_\infty = 0.09$ m s^{-1} shows the transitional region where both generation mechanisms are present and manifested in rapid vertical growth of the fluctuation distribution (also seen in the profiles of figure 6*c*). Additionally, snapshot proper orthogonal decomposition (POD) analysis was performed following Sirovich (1987) on a subset of 1000 fluctuating velocity fields for these three cases. POD is used to extract the dominant spatial features of the flow by decomposing the fluctuating velocity signal $\boldsymbol{u}'(\boldsymbol{x}, t)$ into a deterministic part $\boldsymbol{\phi}^n(\boldsymbol{x})$ (POD modes) and time-dependent coefficients $a^n(t)$ as

$$\boldsymbol{u}'(\boldsymbol{x}, t) = \sum_{n=1}^{1000} a^n(t)\boldsymbol{\phi}^n(\boldsymbol{x}). \tag{3.1}$$

For a more detailed description of POD, the reader is referred to the work of Lumley (1970), Sirovich (1987) and Berkooz, Holmes & Lumley (1993). Figure 8 shows the first three modes of the streamwise velocity fluctuations $\phi_{u'}$ for the two higher free-stream velocities. For the case of $U_\infty = 0.16$ m s^{-1}, the three modes contain 23 % of

https://doi.org/10.1017/jfm.2016.575 Published online by Cambridge University Press

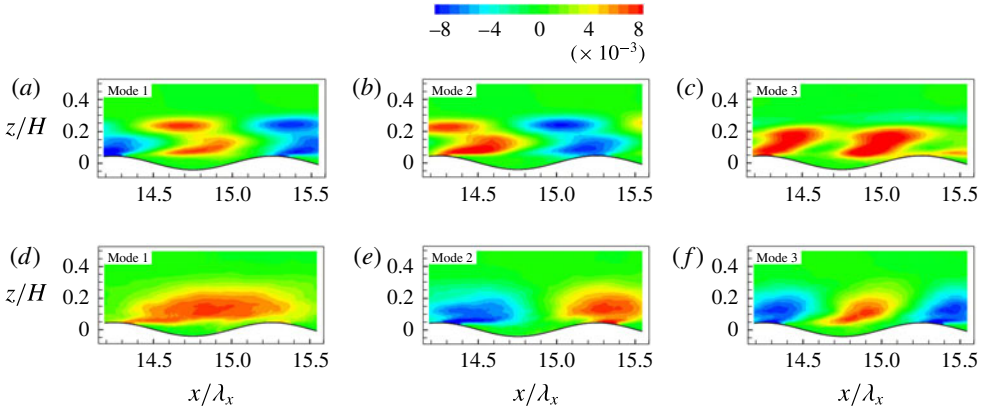


FIGURE 8. POD modes of the streamwise velocity fluctuations ϕ_u' for $U_\infty = 0.09$ m s^{-1} (*a*,*b*,*c*) and $U_\infty = 0.16$ m s^{-1} (*d*,*e*,*f*).

the total energy of all modes and are in agreement with Hamed *et al.* (2015). For the case of $U_\infty = 0.07$ m s^{-1} (omitted here for brevity), the first mode showed a band similar to that observed in the streamwise velocity variance and contributed 80 % of the total energy. The case of interest is $U_\infty = 0.09$ m s^{-1}, where the three modes shown contribute 36 % of the total energy but do not resemble those in the turbulent regime. The spatial structures exhibit different scales and show an interaction between the region away from the wall, which is influenced by the steady disturbances, and structures near the wall, which are influenced by the topography. Finally, it is worth pointing that similar behaviour and energy content were observed in the POD modes for the 2D case in the transitional region.

Figures 5 and 7 highlight the difference in the nature of the transitional region across the two roughnesses. For the 2D case, the narrow band of high velocity variance in the region $4 \lesssim x/\lambda_x \lesssim 4.7$ is associated with the velocity inflection point as discussed above. In the 3D case, the wider band is associated with the velocity deficit region originating from the interaction of the wakes of upstream elements. The rapid vertical growth of the fluctuation distribution is a common feature of the transition region across both roughnesses. The generation of shear layer turbulence in the turbulent region is another common feature (Hamed *et al.* 2015).

4. Conclusions

The transition to turbulence over 2D and 3D roughness was studied experimentally using planar PIV and refractive index matching. The topography covered the entire flow domain, which complements previous works that studied the disturbances created by a short roughness patch (e.g., Downs *et al.* 2008; Kuester & White 2015). The recirculation within the troughs of the 2D roughness facilitates the vertical displacement and growth of the boundary layer over the roughness. However, an inflection point in the displaced boundary layer profile promotes high shear and fluctuations that occur in the region above the roughness. For the 3D topography, the flow transition is significantly delayed ($Re_x = 120\,000$ versus the 50 000 of the 2D case). In the transitional region, the interaction of the wakes of upstream elements is manifested in a deficit in the mean streamwise velocity profile above the roughness. The significant delay in flow transition over the 3D roughness is attributed

https://doi.org/10.1017/jfm.2016.575 Published online by Cambridge University Press

to the spanwise flows within the topography (measured by Hamed *et al.* (2015)), which reduce the likelihood of flow separation (and, consequently, velocity inflection points) by injecting high-momentum fluid in the wakes of the 3D hills. Within the transitional region fluctuations are initially observed above the roughness and are due to the inflection point of the displaced boundary layer for the 2D case and the velocity deficit for the 3D case. These above-roughness disturbances are thought to trigger additional disturbances near the roughness. The above- and near-roughness regions of enhanced mean shear and fluctuations interact, leading to rapid vertical growth of the turbulent fluctuations.

Acknowledgements

This work was supported by the Department of Mechanical Science and Engineering, University of Illinois at Urbana-Champaign, as part of the start-up package of L.P.C. The experiments were performed in a facility built under the National Science Foundation grant award CBET-0923106. The authors are grateful for the help of undergraduate students A. Patkar and D. Harmon at the University of Illinois.

References

BAI, K. & KATZ, J. 2014 On the refractive index of sodium iodide solutions for index matching in PIV. *Exp. Fluids* **55**, 1–6.

BERKOOZ, G., HOLMES, P. & LUMLEY, J. L. 1993 The proper orthogonal decomposition in the analysis of turbulent flows. *Annu. Rev. Fluid Mech.* **25** (1), 539–575.

BERNARDINI, M., PIROZZOLI, S., ORLANDI, P. & LELE, S. K. 2014 Parameterization of boundary-layer transition induced by isolated roughness elements. *AIAA J.* **52** (10), 2261–2269.

BLOIS, G., CHRISTENSEN, K. T., BEST, J. L., ELLIOTT, G., AUSTIN, J., DUTTON, C., BRAGG, M., GARCIA, M. & FOUKE, B. 2012 A versatile refractive-index-matched flow facility for studies of complex flow systems across scientific disciplines. In *50th American Institute of Aeronautics and Astronautics (AIAA) Aerospace Sciences Meeting, Nashville, TN, AIAA Paper* 2012–0736.

CHOI, K. 2006 Fluid dynamics: the rough with the smooth. *Nature* **440** (7085), 754–754.

COSSU, C. & BRANDT, L. 2002 Stabilization of Tollmien–Schlichting waves by finite amplitude optimal streaks in the Blasius boundary layer. *Phys. Fluids* **14** (8), L57–L60.

DOWNS, R. S., WHITE, E. B. & DENISSEN, N. A. 2008 Transient growth and transition induced by random distributed roughness. *AIAA J.* **46** (2), 451–462.

DREWS, S. D. 2012 Direct numerical simulations of flow past quasi-random distributed roughness. Master's thesis, University of Texas at Austin.

DREWS, S. D., DOWNS, R. S., DOOLITTLE, C. J., GOLDSTEIN, D. & WHITE, E. B. 2011 Direct numerical simulations of flow past random distributed roughness. *AIAA Paper* 2011-564.

DRYDEN, H. L. 1953 Review of published data on the effect of roughness on transition from laminar to turbulent flow. *J. Aero. Sci.* **20** (7), 477–482.

EDELMANN, C. A. & RIST, U. 2015 Impact of forward-facing steps on laminar–turbulent transition in transonic flows. *AIAA J.* **53** (9), 2504–2511.

ERGIN, F. G. & WHITE, E. B. 2006 Unsteady and transitional flows behind roughness elements. *AIAA J.* **44** (11), 2504–2514.

FRANSSON, J. H. M., TALAMELLI, A., BRANDT, L. & COSSU, C. 2006 Delaying transition to turbulence by a passive mechanism. *Phys. Rev. Lett.* **96** (6), 064501.

GOLDSTEIN, M. E. 1985 Scattering of acoustic waves into Tollmien–Schlichting waves by small streamwise variations in surface geometry. *J. Fluid Mech.* **154**, 509–529.

HAMED, A. M., KAMDAR, A., CASTILLO, L. & CHAMORRO, L. P. 2015 Turbulent boundary layer over 2d and 3d large-scale wavy walls. *Phys. Fluids* **27** (10), 106601.

https://doi.org/10.1017/jfm.2016.575 Published online by Cambridge University Press

KLEBANOFF, P. S., SCHUBAUER, G. B. & TIDSTROM, K. D. 1955 Measurements of the effect of 2-dimensional and 3-dimensional roughness elements on boundary-layer transition. *J. Aero. Sci.* **22** (11), 803–804.

KLEBANOFF, P. S. & TIDSTROM, K. D. 1972 Mechanism by which a two-dimensional roughness element induces boundary-layer transition. *Phys. Fluids* **15** (7), 1173–1188.

KUESTER, M. S. & WHITE, E. B. 2015 Roughness receptivity and shielding in a flat plate boundary layer. *J. Fluid Mech.* **777**, 430–460.

LUMLEY, J. 1970 *Stochastic Tools in Turbulence*. Academic.

PLOGMANN, B., WÜRZ, W. & KRÄMER, E. 2014 On the disturbance evolution downstream of a cylindrical roughness element. *J. Fluid Mech.* **758**, 238–286.

RESHOTKO, E. 2001 Transient growth: a factor in bypass transition. *Phys. Fluids* **13** (5), 1067–1075.

RESHOTKO, E. & TUMIN, A. 2004 Role of transient growth in roughness-induced transition. *AIAA J.* **42** (4), 766–770.

SHAHINFAR, S., FRANSSON, J. H. M., SATTARZADEH, S. S. & TALAMELLI, A. 2013 Scaling of streamwise boundary layer streaks and their ability to reduce skin-friction drag. *J. Fluid Mech.* **733**, 1–32.

SHAHINFAR, S., SATTARZADEH, S. S., FRANSSON, J. H. M. & TALAMELLI, A. 2012 Revival of classical vortex generators now for transition delay. *Phys. Rev. Lett.* **109** (7), 074501.

SIROVICH, L. 1987 Turbulence and the dynamics of coherent structures. Part I: coherent structures. *Q. Appl. Maths* **45** (3), 561–571.

SMITH, A. & CLUTTER, D. W. 1959 The smallest height of roughness capable of affecting boundary-layer transition. *J. Aero. Sci.* **26**, 229–245.

TANI, I. 1969 Boundary-layer transition. *Annu. Rev. Fluid Mech.* **1** (1), 169–196.

YE, Q., SCHRIJER, F. F. J. & SCARANO, F. 2016 Boundary layer transition mechanisms behind a micro-ramp. *J. Fluid Mech.* **793**, 132–161.

https://doi.org/10.1017/jfm.2016.575 Published online by Cambridge University Press